



**WIRE ARC ADDITIVE MANUFACTURING COMPONENTS FATIGUE LIFE
AND STRESS CONCENTRATION EVALUATION USING FINITE ELEMENT
ANALYSIS**

LANKAAN JA VALOKAAREEN PERUSTUVIEN
SUORAKERROSTUSKAPPALEIDEN VÄSYMISKESTÄVYYDEN JA
JÄNNITYSKESKITTUMIEN ARVIOINTIA KÄYTTÄEN
ELEMENTTIMENETELMÄÄ

Lappeenranta–Lahti University of Technology LUT

Bachelor's Programme in Mechanical Engineering, Bachelor's thesis

2024

Harry Zimmermann

Examiner(s): D.Sc. Kalle Lipiäinen

D.Sc. Shahriar Afkhami

ABSTRACT

Lappeenranta–Lahti University of Technology LUT

LUT School of Energy Systems

Mechanical Engineering

Harry Zimmermann

WIRE ARC ADDITIVE MANUFACTURING COMPONENTS FATIGUE LIFE AND STRESS CONCENTRATION EVALUATION USING FINITE ELEMENT ANALYSIS

Bachelor's thesis

2024

36 pages, 17 figures, 4 tables and 2 appendices

Examiner(s): Kalle Lipiäinen, D.Sc. (tech), Shahriar Afkhami, D.Sc. (tech)

Keywords: additive manufacturing, direct energy deposition, WAAM, DED-arc, fatigue, FEA, finite element method, TCD, theory of critical distances, surface quality, stress concentration

This thesis explores the fatigue performance of wire arc additive manufacturing components, with an emphasis on the effects of surface quality on fatigue performance. This thesis consists of a literature review and an experimental part. The literature review discusses WAAM and its applications as well as its fatigue behavior, highlighting the effects of poor surface quality on the fatigue performance of as-built WAAM components. In the experimental part, six as-built WAAM components made with high strength X96 steel filler wire will be evaluated for their fatigue performance using finite element analysis, the theory of critical distances and uniaxial fatigue tests.

The fatigue tests resulted in FAT classes of 151MPa with a slope of $m=4.25$ and 110MPa with a slope of $m=3$. The finite element analysis and the theory of critical distances resulted in an average fatigue notch factor of 1.77.

TIIVISTELMÄ

Lappeenrannan–Lahden teknillinen yliopisto LUT

LUTin energijärjestelmien tiedekunta

Konetekniikka

Harry Zimmermann

LANKAAN JA VALOKAAREEN PERUSTUVIEN SUORAKERROSTUSKAPPALEIDEN VÄSYMISKESTÄVYYDEN JA JÄNNITYSKESKITTUMIEN ARVIOINTIA KÄYTTÄEN ELEMENTTIMENETELMÄÄ

Konetekniikan kandidaatintyö

2024

36 sivua, 17 kuvaa, 4 taulukkoa ja 2 liitettä

Tarkastaja(t): TkT Kalle Lipiäinen, TkT Shahriar Afkhami

Avainsanat: lisäävä valmistus, suorakerrostus, WAAM, väsyminen, FEA, elementtimenetelmä, TCD, pinnan laatu, jännitys konsentraatio

Tämä kandidaatin työ tutkii lankaan ja valokaareen perustuvalla suorakerrostusmenetelmällä tuotettujen kappaleiden väsymiskestävyttä painottaen pinnan laadun vaikutusta väsymiskestävyteen. Tämä työ koostuu sekä kirjallisuuskatsauksesta että kokeellisesta osuudesta. Kirjallisuus katsauksessa käsitellään lankaan ja valokaareen perustuvaa suorakerrostusmenetelmää ja sen sovelluksia sekä sen väsymisominaisuuksia korostaen heikon pinnanlaadun vaikutuksia kappaleiden väsymiskestävyteen. Kokeellisessa osuudessa tutkitaan kuuden lujasta X96 täytelangasta lankaan ja kaareen perustuvalla suorakerrostuksella valmistetun kappaleen väsymiskestävyttä käyttäen elementtimenetelmää, kriittisten etäisyyksien teoriaa (theory of critical distances) ja uniaksiaalisia väsymiskokeita.

Väsymiskokeet johtivat FAT luokkiin 151MPa kulmakertoimella $m=4.25$ ja 110MPa kulmakertoimella $m=3$. Elementtimenetelmällä ja kriittisten etäisyyksien teorialla saatiin lovenvaikutuslukujen keskiarvoksi 1.77.

SYMBOLS AND ABBREVIATIONS

Roman

R_a	arithmetic mean height for roughness profile	[μm]
R_z	Maximum peak to valley distance for roughness profile	[μm]
W_a	arithmetic mean height for waviness profile	[mm]
W_z	Maximum peak to valley distance for waviness profile	[mm]
P_a	arithmetic mean height for primary profile	[mm]
P_z	Maximum peak to valley distance for primary profile	[mm]
K_t	Stress concentration factor (SCF)	
K_f	Fatigue notch factor	
ΔK_{th}	Fatigue crack propagation threshold	
$R_{p0.2}$	Yield strength	[MPa]
R_m	Ultimate tensile strength	[MPa]
F	Force	[N]
F_a	Force amplitude	[N]
F_R	Load range	[N]
L	Critical distance	[mm]
a	Critical distance value for point method	[mm]
N	Number of cycles	
N_f	Number of cycles till failure	
N_{if}, N_{ic}	Nesting index	
l_e	Surface profile length	[mm]
E	Young's modulus	[GPa]
ν	Poisson's ratio	

m	Slope for FAT class	
C	Fatigue strength coefficient	
Greek		
σ	Stress	[MPa]
σ_{nom}	Nominal stress	[MPa]
$\sigma_{max,prn}$	Maximum principal stress	[MPa]
$\Delta\sigma$	Cyclic stress range	[MPa]
σ_{eff}	Effective stress	[MPa]
$\Delta\sigma_0$	Critical cyclic stress	[MPa]
ρ	Mass density	[g/cm ³]

Abbreviations

FEA	Finite Element Analysis
FEM	Finite Element Method
AM	Additive Manufacturing
AB	As built
DED	Direct Energy Deposition
WAAM	Wire Arc Additive Manufacturing
GMAW	Gas Metal Arc Welding
GTAW	Gas Tungsten Arc Welding
PAW	Plasma Arc Welding
SW	Surface Waviness
SCF	Stress Concentration Factor
TCD	Theory of Critical Distances
PM	Point Method

FAT

Fatigue strength at 2-million-cycles

Table of contents

Abstract

(Symbols and abbreviations)

1	Introduction	8
1.1	Research problem	8
1.2	Research objective and questions	9
1.3	Research methods and scope	9
2	WAAM technology and its applications	10
3	The fatigue performance of WAAM components.....	12
3.1	Surface quality and its relation to fatigue	12
3.1.1	Surface profiles and parameters.....	13
3.1.2	Previous research	15
3.2	Theory of Critical Distances for fatigue evaluation – Point Method.....	16
4	Research methods.....	17
4.1	Test specimen preparation	17
4.2	3D-scanning and surface profile evaluation	18
4.3	Finite element analysis.....	21
4.4	Theory of critical distances – Point method	23
4.5	Fatigue testing.....	24
4.6	S-N curves.....	26
5	Results	27
6	Discussion.....	30
6.1	Key findings and comparison to previous research	30
6.2	Reliability and validity.....	31
6.3	Conclusions.....	32
	References.....	33

Appendices

Appendix 1. The code used in FEMAP API to import the surface profile data.

Appendix 2. FEA models.

1 Introduction

Additive manufacturing (AM) is a process where parts are produced by adding material layer by layer based on 3D model data (SFS-EN ISO/ASTM 52900:2021). It is a fast-growing industry that has caught lots of attention due to its capabilities in creating complex shapes with little material wastage and fewer steps in production compared to many of the traditional methods found in subtractive manufacturing (Garner L, 2023; Dutta, Babu and Jared 2019, 3). With the improved use of metals in additive manufacturing, the process has been able to expand its applications from a more prototype-based production to further industrial applications and manufacturing (Afkhami et al., 2021). One of the trending processes in metal additive manufacturing, especially when it comes to larger and faster additive production, is a process called direct energy deposition (DED). Direct energy deposition is a process of additive manufacturing, where material, typically metal, is melted by a directed heat source while being deposited on to a build surface (SFS-EN ISO/ASTM 52900:2021). DED covers a wide range of methods which can be further subcategorized depending on their heat source, material feedstock and feed principle and in this thesis, we will be focusing on a subcategory called wire arc additive manufacturing (WAAM), which is also known as DED-arc. WAAM is a process based on arc-welding where the part is formed layer-by-layer with continuous welds. It has the highest deposition rates of all metal additive manufacturing methods, however it typically also has a lower print resolution and poor as-built surface quality, which can have significant effects on its fatigue performance.

1.1 Research problem

While there has been a growing number of research on the mechanical and fatigue properties of WAAM components, the existing research on the fatigue performance of WAAM is still lacking (Gardner L, 2023; Becker et al., 2021) and due to the complicated nature of fatigue and the many fatigue affecting factors in WAAM, some of the previous research may be difficult or impossible to implement. Here fatigue refers to the weakening of material properties under cyclic stress and it is the most significant cause of failure in metal structures and mechanical parts (Bathias and Pineau, 2010) (Murakami, 2019) which is why it is

important to understand thoroughly for non-destructive design, effective implementation of different WAAM technologies in different applications and to help choose suitable post-processing methods. There are many factors in WAAM which can influence its fatigue performance. These factors include but are not limited to high temperatures, production speeds, print directions and materials, all of which can affect the fatigue performance of produced parts by causing changes in surface quality, porosity, defects, residual stresses, anisotropy and microstructures (Becker et.al 2021). This added complexity makes it more difficult to implement previous research and is a reason why more research is required.

1.2 Research objective and questions

The objective of this thesis is to use the theory of critical distances (TCD) with Finite Element Analysis (FEA) as well as fatigue tests to evaluate the fatigue performance of as-built high strength X96 WAAM components. This thesis aims to answer the research questions listed below:

- What is the fatigue strength of WAAM components made from high strength X96 steel wire?
- How effectively can TCD and FEA be used to estimate the fatigue performance of as built WAAM components?

1.3 Research methods and scope

This thesis is made up of a literature review and an experimental part. The literature review will examine the theory behind WAAM technologies as-well as fatigue and its relation to surface quality. The literature review will also focus on previous research on the effects of surface quality on fatigue properties of WAAM parts. In the experimental part, test specimens will be made with WAAM using Böhler Union X96 high strength filler-wire, which will then be 3D-scanned and imported to finite element analysis software - FEMAP, where 2D-FEA will be used along TCD for fatigue life and stress concentration evaluation. Uniaxial fatigue tests will also be performed for the as-built specimens and the results will be compared with FEA and TCD as well as the literature review findings.

2 WAAM technology and its applications

Wire arc additive manufacturing (WAAM) is a method of direct energy deposition (DED) which uses an arc as its heat source and metal wire as its feedstock. It is based on a concept similar to arc welding, and similarly to arc welding WAAM can be further categorized depending on the arc technology used, such as gas metal arc welding (GMAW), gas tungsten arc welding (GTAW) and plasma arc welding (PAW) (Evans et al., 2022; Shah et al., 2023). GMAW is a method, which unlike the other methods, uses filler wire as its electrode which is fed onto the build surface creating an arc and a melt pool. GTAW and PAW on the other hand use separate feeding and a non-consumable electrode however they differ from each other in nozzle structure and arc location. In PAW the arc is formed inside the nozzle chamber unlike GTAW where the arc is formed outside the nozzle. This causes PAW to have a more focused arc, with more heat and precision, however also creating the need for nozzle chamber cooling which is typically done by running water through copper wires in the nozzle chamber. Some of the different features for these WAAM technologies are listed in Table 1.

Table 1: WAAM processes and key features (Salunkhe, Amancio-Filho and Davim, 2023; Singh, 2016; Wu et al., 2018).

WAAM process	Electrode	Wire Feed	Typical deposition rate
GMAW	Filler wire	Consumable wire electrode	3 - 4 kg/h
GMAT	nonconsumable Tungsten	Separate wire feed	1 - 2 kg/h
PAW	nonconsumable Tungsten	Separate wire feed	2 - 4 kg/h

WAAM can achieve the highest deposition rates of all metal additive manufacturing methods with stated deposition rates of up to 9.5kg/h (Martina et al., 2019), however this was done using tandem WAAM and more commonly deposition rates vary between 1kg/h and 4kg/h when using single source WAAM processes (Salunkhe, Amancio-Filho and Davim, 2023; Tomar, Shiva and Nath, 2022) as can be seen in Table 1. Out of the different types of WAAM processes, GMAW has been found to have highest deposition rates with two to three times faster deposition than GTAW or PAW (Wu et al., 2018; Tomar, Shiva

and Nath, 2022). These high deposition capabilities of WAAM processes are one of the key features which make WAAM such a trending additive manufacturing method.

WAAM processes are typically controlled by either a CNC machine or a robot arm and a build platform. Using a robot arm allows for larger fabrication due to fewer dimensional restrictions which a CNC machine might have. It is also possible to use multiple robot arms for one WAAM project allowing for even larger and faster fabrication. One of the down sides to high deposition rates of WAAM is a decrease in geometric accuracy and surface quality when compared to other metal AM, which is why post processing is typically required (Tomar, Shiva and Nath, 2022; Evans et al., 2022). This issue may however also be addressed using a hybrid-WAAM process where additional machining is used along WAAM manufacturing to get the desired geometry and build quality (Shah et al., 2023).

In addition to the high deposition rates and large fabrication capabilities, WAAM may also have economic benefit, when compared to other metal AM methods. In a study by Cunningham et al. 2017, parts made from Ti6Al4V using WAAM were found to be the most cost-effective metal AM method with a cost reduction of about 20-45% when compared to electron beam additive manufacturing and 69-79% when compared to direct metal laser sintering.

So far WAAM has found applications and growing interest in several industries such as aerospace, marine and automotive (Tomar, Shiva and Nath, 2022). In a review by Pant et al., 2023, WAAM was found to have noticeable capabilities in aerospace manufacturing, which typically requires complex structures with strong lightweight metals such as titanium alloys. In the review WAAM showed promising results for optimized lightweight structures to be manufactured with few production steps and with relatively low production costs, due to low material waste and near-net-shape fabrication. This was also supported by a review from Lin, Song and Yu, 2021, which investigated the applications of titanium alloys in WAAM. In 2020, Ziółkowski and Dyl reviewed the use of AM in shipbuilding, where WAAM could be found used efficiently in for example marine propeller manufacturing. WAAM has also gained interest in structural engineering, where it benefits from large fabrication capabilities, fast deposition and optimizable structures (Gardner, 2023). For example, a 12-meter-long stainless-steel footbridge was made in a project led by MX3D using WAAM, which presents some capabilities of WAAM in practical structural applications (MX3D).

3 The fatigue performance of WAAM components

Fatigue is a phenomenon where material weakens under repetitive fluctuating stress due to the initiation and propagation of cracks which if continued eventually leads to failure. Fatigue is known to be one of the leading causes of mechanical failures, owning up to about 80-90% of all mechanical failure cases and it is especially difficult to predict because it typically occurs under stresses significantly lower than in the case of purely static failure. (Nussbaumer et al, 2018; Bathias & Pineau, 2010; Murakami, 2019)

There are several factors which may cause as-built WAAM components to have lower fatigue performance compared to traditionally manufactured parts. For example, as-built WAAM parts often have worse surface quality in comparison to traditionally manufactured components and they are subjected to high temperature fluctuation which causes residual stresses and anisotropy. During the melting and solidification phase, defects such as porosity might also occur due to gas getting trapped in the molten material, which causes a decrease in fatigue performance, however porosity in WAAM can be highly influenced with proper parameters (Sandeep et al., 2022). (Gardner, 2023) It is important to understand just how much fatigue performance is altered by these different factors in WAAM produced part for non-destructive designs and when considering post-processing.

3.1 Surface quality and its relation to fatigue

Surface quality has been known to have a potentially significant influence on the fatigue performance of AM components (Garner L, 2023; Gockel et al, 2019), which is especially true for WAAM components which tend to have the worst surface quality in their as-built form when compared to other metal AM or traditional manufacturing. This relationship with surface quality and fatigue is due to the tendency of fatigue cracks initiating from the surface of the components. This is because surface deviations act as local stress risers in the component, which may then work as sources for fatigue cracks, thus lowering fatigue performance. (Bathias & Pineau, 2010; Murakami, 2019) The surface quality may have noticeable differences even between different WAAM parts may, depending on which WAAM technology, material and parameters are used, where typically, higher deposition

rates and higher energy input relate to a decrease in surface quality. Additionally, a material specific notch sensitivity value, q , influences how much the materials fatigue performance is affected by stress concentrations. Typically, brittle materials have higher notch sensitivity and ductile materials on the other hand have lower notch sensitivity. (Pilkey et al, 2020)

WAAM components, like other DED methods, are manufactured in a layer-by-layer nature which causes wave-like surface unevenness as well as smaller surface profile irregularities from the welding process resulting in a generally poor surface quality.

3.1.1 Surface profiles and parameters

There are many useful parameters to describe the quality of a surface profile and several sub-profiles can be isolated from the primary surface profile to describe certain specific qualities of the profile. Here the primary surface profile is the surface profile data acquired from some surface profile measuring device, for example a 3D-profilometer, and it includes both the form and the primary profile of the surface. Here form basically describes the basic nominal shape of the surface, so for example if it's a circular shape or a crooked line for a 2D surface profile and the primary profile describes the undulations of the profile, so its waviness and roughness. The form removal operation, also known as levelling, is called an F-operation and it can be done by use of operation total least square fit (SFS-EN ISO 21920-3:2022). The form removal gives the primary profile, which shows all the surface undulations in a levelled state. The primary profile can be further filtered into waviness and roughness profiles, where waviness can be described as the larger undulations, where the smaller scale irregularities are filtered out and on the contrary roughness can be described as the smaller undulations where the larger waves are filtered out. (SFS-EN ISO 21920-2:2022) This difference between waviness and roughness can be seen in Figure 1.

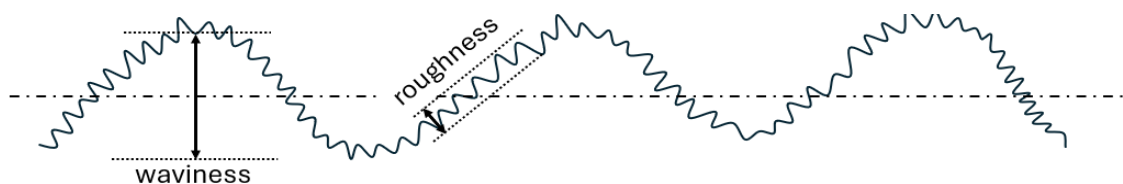


Figure 1: Shows the difference between waviness and roughness on an imaginary profile.

The schematic process of deriving the primary profile (P), waviness profile (W) and roughness profile (R) can be seen in Figure 2, where the nesting indexes N_{if} and N_{ic} are

values used to control the filtering, for example the cut-off wavelength for Gaussian filtering method (SFS-EN ISO 21920-2:2022).

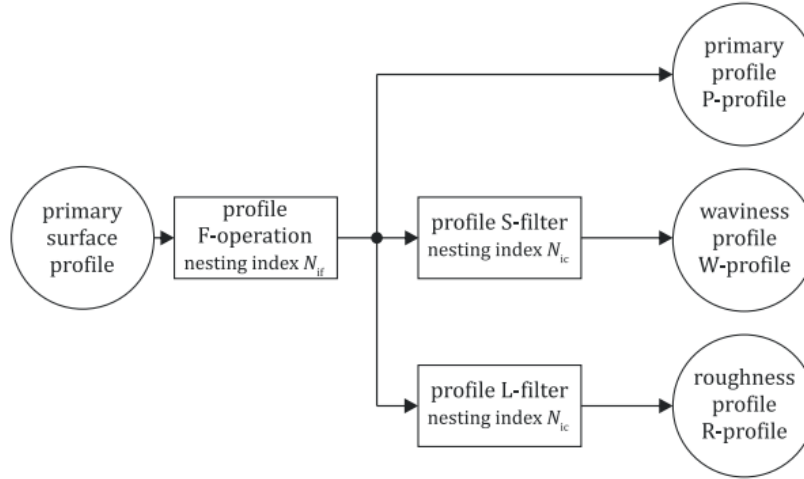


Figure 2. This image illustrates how the different profiles are derived from the primary surface profile (SFS-21920-2:2022).

Several parameters can be calculated from the primary, waviness and roughness profiles and despite the technical differences of these profiles, the same mathematical formulas can typically be applied to all of the different profiles, where the difference in output obviously comes from the profiles having different data points due to the filtering. Common parameters for the profiles include the arithmetic mean heights R_a , W_a and P_a (equation 1) and the total heights R_z , W_z and P_z also called the maximum peak to valley distance (equation 2). (SFS-EN ISO 21920-2:2022)

$$R_a, W_a, P_a = \frac{1}{l_e} \int_0^{l_e} |z(x)| dx \quad (1)$$

$$R_z, W_z, P_z = \max(z(x)) - \min(z(x)) \quad (2)$$

Where x describes the profile length coordinates and z describes the height coordinates.

It should be noted here before the next section that some of these parameters may be found in some cases used ambiguously in the literature, which is why it is advisable to see how the value was derived in the original source in case of confusion.

3.1.2 Previous research

So far, several studies have found clear decreases in fatigue performance of as-built WAAM parts compared to similarly built parts with surface post-processing. Huang et al found in their 2023 study that as-built WAAM manufactured plates made with ER70S-6 steel wire had about 35% reduction in fatigue life based on nominal stress analysis when compared to parts with a machined surface. Similar results were concluded in a study by Dirisu et al., in 2020, where ER70S-6 WAAM as-built specimens with surface waviness value of about 0.18mm were compared to specimens with rolled and machined surfaces. Here both machining and rolling had clear improving effects on fatigue performance compared to as-built specimens, with the machined specimens performing best overall. A study by Bartsch et al., 2021, compared the fatigue performance of single wire WAAM technology parts which had max surface roughness values of about 0.610 mm, with three wire WAAM technology parts which had max surface roughness values of about 2.112 mm both using G3si1 filler wire. They found surface roughness to be the prevailing factor in the fatigue performance of the examined parts with lower surface roughness correlating with a clear increase in fatigue performance. Another study, done by Hietala et al. in 2023, found that as-built WAAM 316L stainless steel parts with R_a of 0.219mm had about 95-100MPa lower fatigue limit when compared to similarly produced parts with a polished surface with R_a of $0.24\mu\text{m}$ and a milled surface with R_a of $0.55\mu\text{m}$ respectively. Here the decrease in fatigue performance of the polished surface compared to the milled surface was explained by residual stresses caused by the polishing process. (Hietala et al., 2023) A study by Shamir et al., 2023, compared different approaches to estimating the bending fatigue life of WAAM made with titanium alloy Ti-6Al-4V. The study found as-built specimens to have roughly half the bending fatigue life when compared to machined specimens, but it also found the fracture mechanics approach to be a more accurate method for estimating fatigue life in this case when compared to notch fatigue approach. (Shamir et al., 2023) The effects of building position on surface quality and fatigue properties of WAAM were studied by Hensel et al. in 2023. This study found that specimens fabricated in a horizontal 75-degree angle showed a clear decrease in both surface quality and fatigue performance when compared to specimens fabricated on a vertically with no angle. (Hensel et al., 2023)

3.2 Theory of Critical Distances for fatigue evaluation – Point Method

The theory of critical distances (TCD) is formed of a group of different approaches which can be used to predict brittle fractures and fatigue limits for parts with stress concentrations such as notches or notch-like defects which can be found in WAAM components. For example, Lipiäinen et al. used the theory of critical distances in their 2022 research to evaluate the fatigue performance notched and hot-dip galvanized steel components. The theory roots back to the early to mid-nineteen hundreds where it was originally worked on by Neuber and Peterson and has since been influenced by several researchers with Taylor developing it to its current form. TCD is formed of four different approaches which are the point method (PM), the line method (LM), the area method (AM) and volume method (VM), and while these approaches have clear practical differences, they all abide to a material specific critical distance L . (Taylor, 2007) In the case of fatigue, the critical distance L can be solved as a function of two material constants which are the fatigue crack propagation threshold ΔK_{th} and the cyclic critical stress $\Delta\sigma_0$. The critical distance can be described by the following equation.

$$L = \frac{1}{\pi} \cdot \left(\frac{\Delta K_{th}}{\Delta\sigma_0} \right)^2 \quad (3)$$

In this thesis the focus will be on the point method, which is the simplest form of TCD, and it uses the idea that fatigue failure will occur once the stress measured at a certain critical distance value $a = L/2$ from the notch root exceeds the materials cyclic critical stress $\Delta\sigma_0$, i.e. the materials plain fatigue limit. Keep in mind that the critical distance value a is exclusive to the PM and should not be mixed with the general critical distance L . (Taylor, 2007) The point method is described by the following equation.

$$\Delta\sigma(a) = \Delta\sigma_0 \quad (4)$$

The critical distance L may be challenging to solve via equation 2 due to the complexity of assessing the fatigue crack propagation threshold ΔK_{th} . Karakaş, Leitner and Tüzün, 2022 have however proposed a critical distance value of $\frac{L}{2} = 0.1\text{mm}$ for as-built high strength welded steels.

4 Research methods

This thesis was made with a triangulation principle, which was based on three separate methods which were a literature review, fatigue tests and numerical analysis consisting of finite element analysis with the theory of critical distance. In the literature review the current state of WAAM technologies and their applications were presented as well as the fatigue performance of WAAM and how surface quality effects it. The research used in the literature review was searched and acquired through LUT Primo. The research regarding surface quality effects on fatigue performance of wire arc additive manufacturing were primarily selected as peer-reviewed articles from recent years. Most of the sources in the literature review were from the last five years and only a couple sources which dealt about more well-established concepts regarding fatigue or surface quality were over ten years old.

4.1 Test specimen preparation

The test specimens were manufactured in LUT – welding laboratory, using GMAW based WAAM with an ABB robot arm and welding parameters which can be seen in Figure 3. The specimens were made using Böhler Union X96 ultra-high-strength steel filler-wire. Union X96 filler wire in its untreated state has a yield strength of $R_{p0.2} = 930 \text{ MPa}$ and an ultimate tensile strength of $R_m = 980 \text{ MPa}$ (Voestalpine Böhler Welding, 2024).

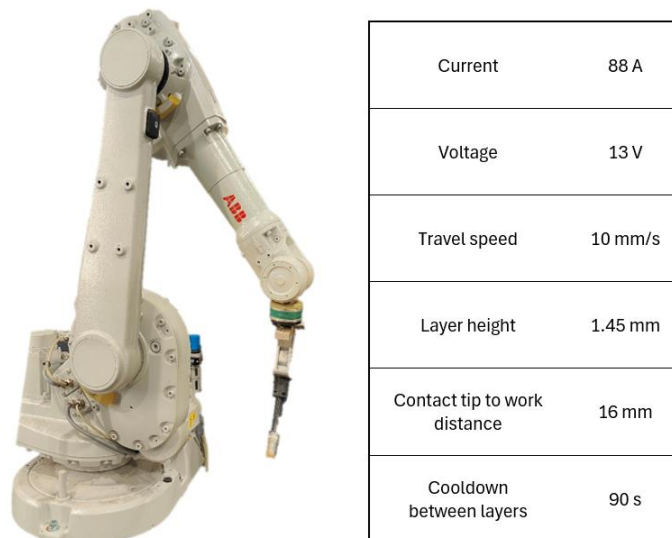


Figure 3: Robot arm and WAAM parameters used for X96 specimen fabrication.

The specimens were prepared by first making a plate like structure which was then cleaned and cut into 125x25 mm specimens with an average thickness of roughly 5 mm. The preparation of the test specimens can be seen in Figure 4. The specimens were finally machined into dog bone shapes which were used in the fatigue tests, however this cannot be seen in any figure.



Figure 4: Presents the preparation of test specimens from WAAM plate.

4.2 3D-scanning and surface profile evaluation

Three different test specimens were used for the scanning and out of those three specimens, different areas and lengths were scanned with an emphasis on scanning areas with the seemingly worst surface quality. The test specimens were scanned using an optic 3D-profilometer, which can be seen in Figure 5. The machine works by directing light from two sources, both of which come in a 35-degree angle unto the specimen from which the light is then reflected back up into the profilometer.



Figure 5: Presents the 3D profilometer which was used to scan the test specimens.

The 3D-profilometer provided data on the surface profiles of the test specimens, which can be seen in Figure 6. The scans were made by creating a line between two selected points from which a 2D-surface profile was then created by the profilometer.

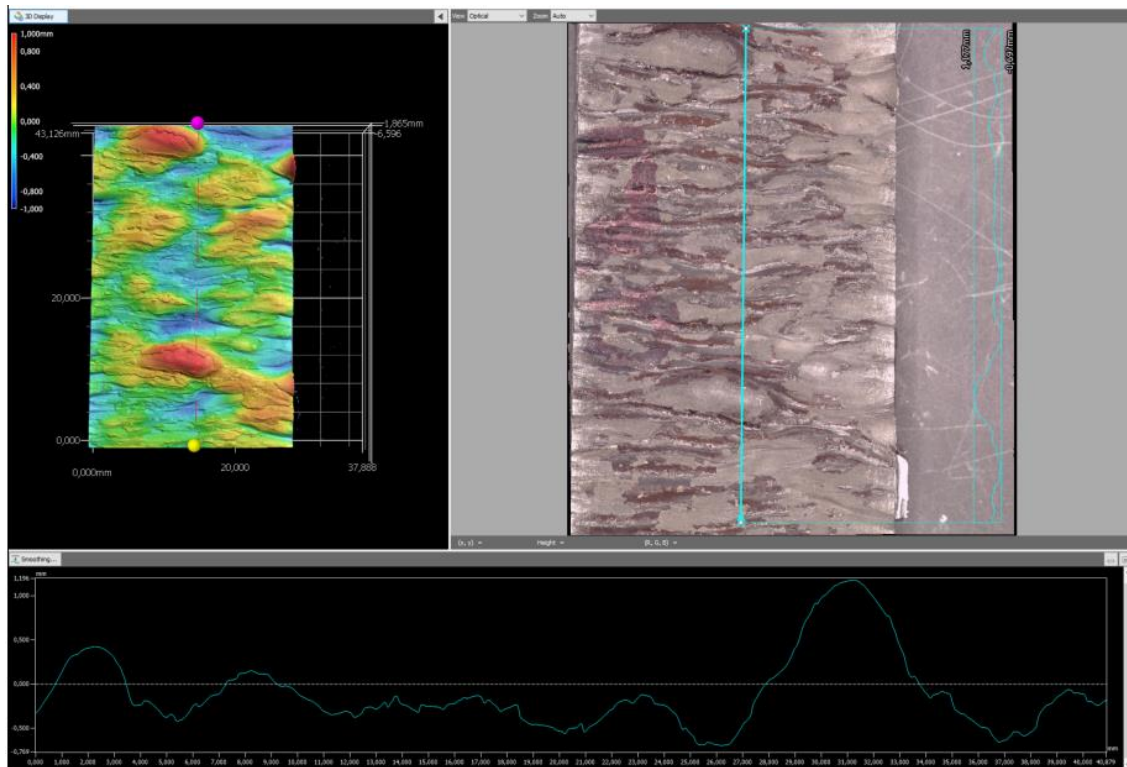


Figure 6. Shows the gathering of surface profile data with a 3D-profilometer.

The 2D-surface data was then saved as an csv-file which could be then used in Microsoft Excel. In Excel, the 2D-surface data points were shown as only x and z coordinate points in separate x and z columns and so a y-axis column was manually added with all zero values for the data to be later made into 2D-finite element analysis. Additionally, all the coordinate rows, consisting of x-, y- and z-coordinates were given ID-numbers manually. The gathered surface data was also used in creating the P, W and R profiles, as well as the parameters for those profiles, which was explained in section 3.1.1 To get the primary profile from the primary surface profile, the form was firstly removed. This could be done simply by creating a linear trendline in Excel from the primary surface profile data points and then subtracting the trendlines z-values from the primary surface profile, giving the primary profile. The waviness and roughness profiles were then filtered from the primary profile using Gaussian filtration in MATLAB with help of standard SFS-EN ISO 16610-21 and ISO 4287-1997. Figure 7 shows the primary surface profile, primary profile, waviness profile and roughness profile and the schematic process of how they were derived.

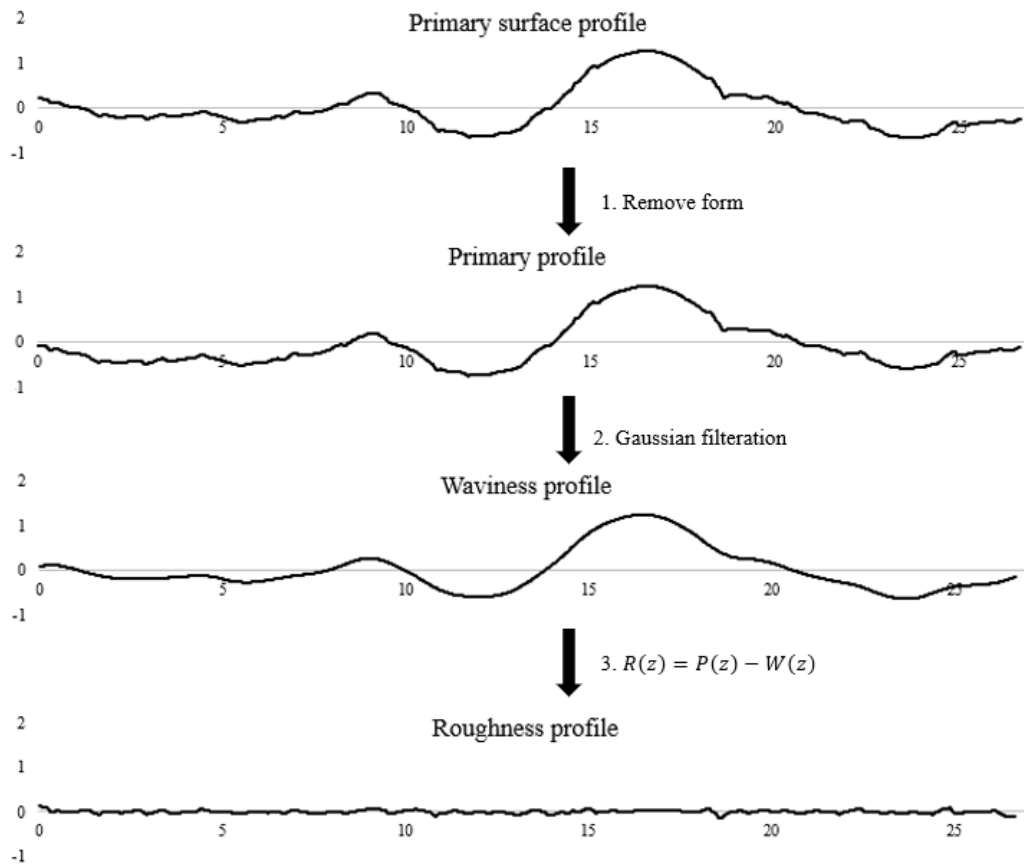


Figure 7. This figure shows how the different surface profiles were derived in this thesis.

After separating the different profiles from each other, the arithmetic mean heights R_a , W_a and P_a as well as the total heights R_z , W_z and P_z were calculated using equations (1-2), from section 3.1.1.

4.3 Finite element analysis

The finite element analysis was made using FEMAP software. First the surface profile data points, which were gathered into Excel as explained in section 4.2, were imported into FEMAP using the FEMAP API programming interface. An example of the code used in FEMAP API can be seen in Appendix 1 Figure 13. After this the surface profile was given a nominal height of roughly 5mm by manually adding two bottom corner points and connecting them to each other and the surface profile with manually added lines. For longer parts the area was divided into segments in order to create a boundary surface (see Figure 8), because FEMAP only allows for a certain number of points to be made into a boundary surface. After this the material properties $E = 210 \text{ GPa}$, $\nu = 0.3$ and $\rho = 7.85 \text{ g/cm}^3$

were added to the part, where E is Young's modulus, ν is Poisson's ratio and ρ is mass density. The part was given a continuous longitudinal load of $80N$ onto one side creating a nominal stress of $80 MPa$. The other non-loaded side was fixedly constraint, and the loaded side was allowed only longitudinal transition. The smooth bottom side was given a constraint allowing only longitudinal transition, because in a real case the component would have roughness of similar magnitude on both sides and the amplifying effect on stress from having roughness on only one side would be evened out. The models where however tested both ways, with the bottom being unconstrained and by allowing only longitudinal transverse and the latter was indeed more accurate. After this the mesh was created using FEMAP auto mesh tool with an element size of $0.01mm$. This element size was found to be accurate in describing stress concentrations in fine details and it was also suitable for the upcoming calculations which are described in section 4.4 After meshing a static analysis was done for the part along with some additional postprocessing. In this analysis the interest was in finding out the principal stresses in the surface profile undulations. The workflow of the finite element analysis can be seen Figure 8.

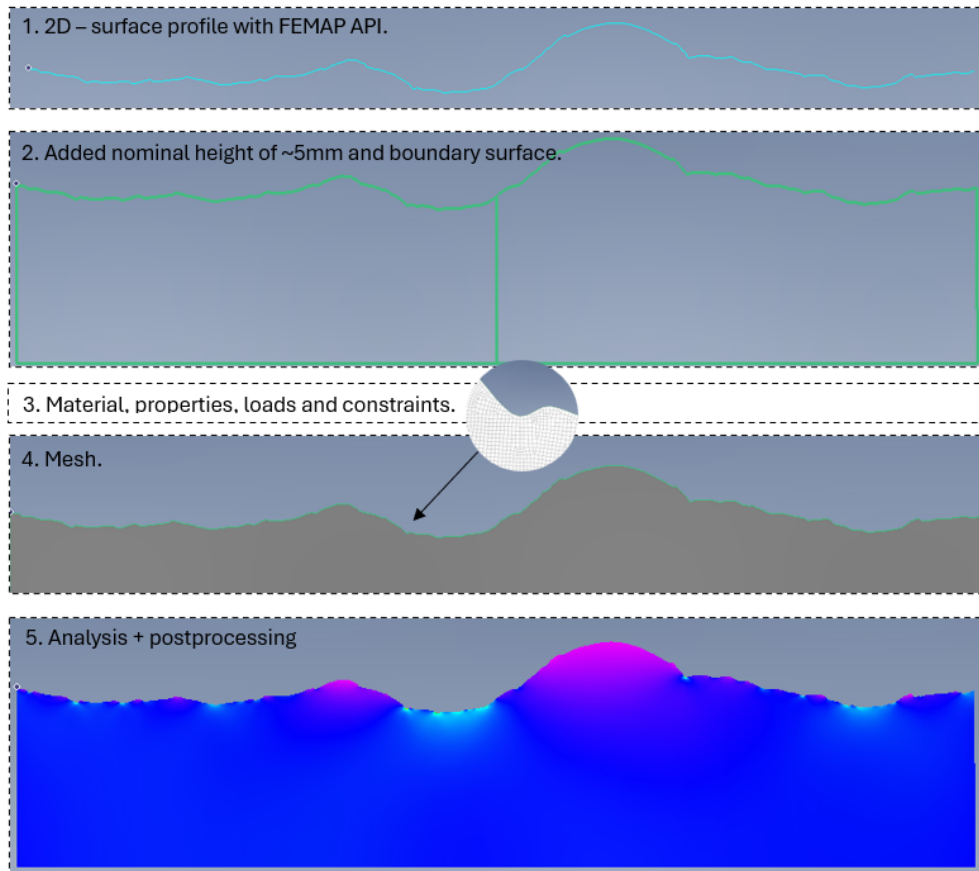


Figure 8. This figure shows the simplified steps in creating FEA for X96 specimens.

4.4 Theory of critical distances – Point method

The point method, which was briefly introduced in section 3.2 was used for assessing the fatigue performance of WAAM X96 finite element models. Since the critical distance value is complicated to solve via equation 2, due to the complicated nature of defining ΔK_{th} , a critical distance value of $\frac{L}{2} = 0.1\text{mm}$ was used for fatigue evaluation as proposed by Karakaş, Leitner and Tüzün in 2022 and Baumgartner et al., 2015 for as-built welds. The stress at critical distance was evaluated by importing element stress data from FEMAP to Excel along with distance measurements from those elements to the stress concentration root. In excel a graph was made from the gathered data describing the stress at a given distance from the max stress which allowed the stress at distance $\frac{L}{2} = 0.1\text{mm}$ to be interpolated using Excel FORECAST function, and because an element size of 0.01mm was used in the meshing, the interpolation could be done accurately. Figure 9 shows the stress along distance from notch root.

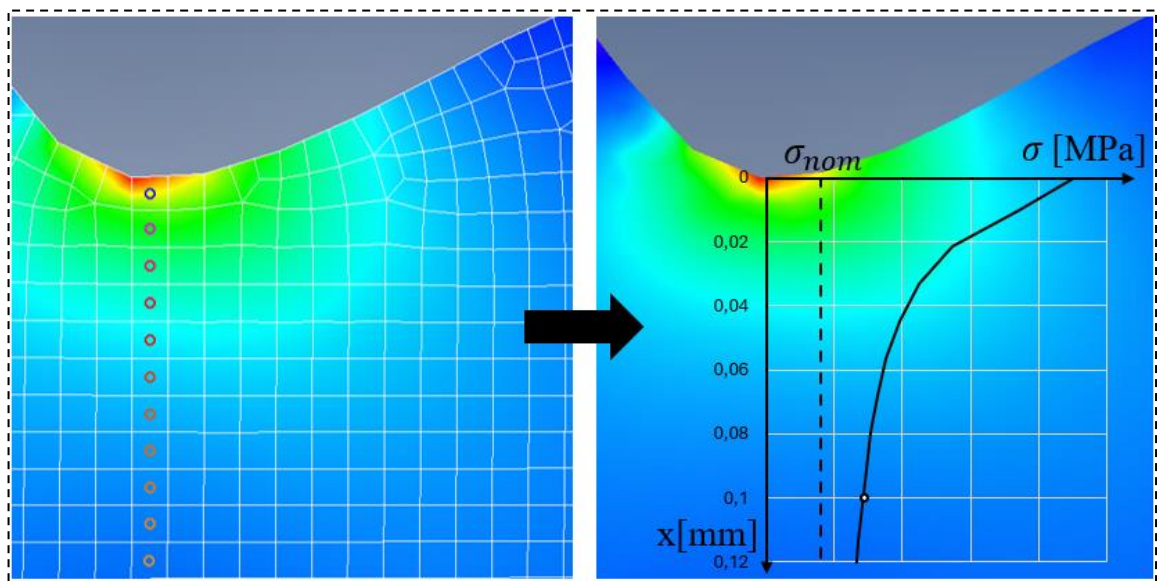


Figure 9. The evaluation of stress at critical distance

In order to evaluate the fatigue performance of the as-built components the stress concentration factor K_t and fatigue notch factor K_f were solved based on the FEA model and PM. Firstly, for clarity reasons, the principal stress at the critical distance $\frac{L}{2}$ obtained from FEA will be referred to as the effective stress (Baumgartner et al., 2015).

$$\sigma_{eff} = \sigma(L/2) \quad (5)$$

Next, the stress concentration factor (SCF) K_t was assessed, which in this case describes the maximum principal stress $\sigma_{max,prn}$ found in the FEA in relation to the components nominal stress σ_{nom} .

$$K_t = \frac{\sigma_{max,prn}}{\sigma_{nom}} \quad (6)$$

Furthermore, according to PM, fatigue failure occurs once the principal stress at a critical distance $\sigma(L/2)$ is equal to the materials plain fatigue limit σ_f , which makes it possible to evaluate the as-built components fatigue limit by finding the nominal stress σ_{nom} at which the statement is true (Taylor, 2007). With linear FEA the previous statement allows for a fatigue notch factor K_f to be assessed based on the relation of σ_{eff} and σ_{nom} as shown by Zhang, 2012. Here it may be explained so that as the locally occurring effective stress reaches the plain material fatigue limit $\sigma_{f,plain}$, the component will undergo fatigue damage and thus the nominal stress at which this happens would be the notched specimens fatigue limit $\sigma_{f,notched}$.

$$K_f = \frac{\sigma_{f,plain}}{\sigma_{f,notched}} \quad (7)$$

$$K_f = \frac{\sigma_{eff}}{\sigma_{nom}} \quad (8)$$

4.5 Fatigue testing

The fatigue tests were made with the WAAM X96 test specimens and the tests were performed in LUT laboratory of steel structures. The fatigue tests were performed with a hydraulic test machine, which can be seen in Figure 10. The test was performed with purely axial cyclic tensile loading with a constant amplitude load. The loading for each fatigue test can be seen in Table 2. The coupon labelling in Table 2 begins with the type of testing (F=Fatigue), then the material (X96), followed by type of coupon (AB=as built) and finally an ID number.

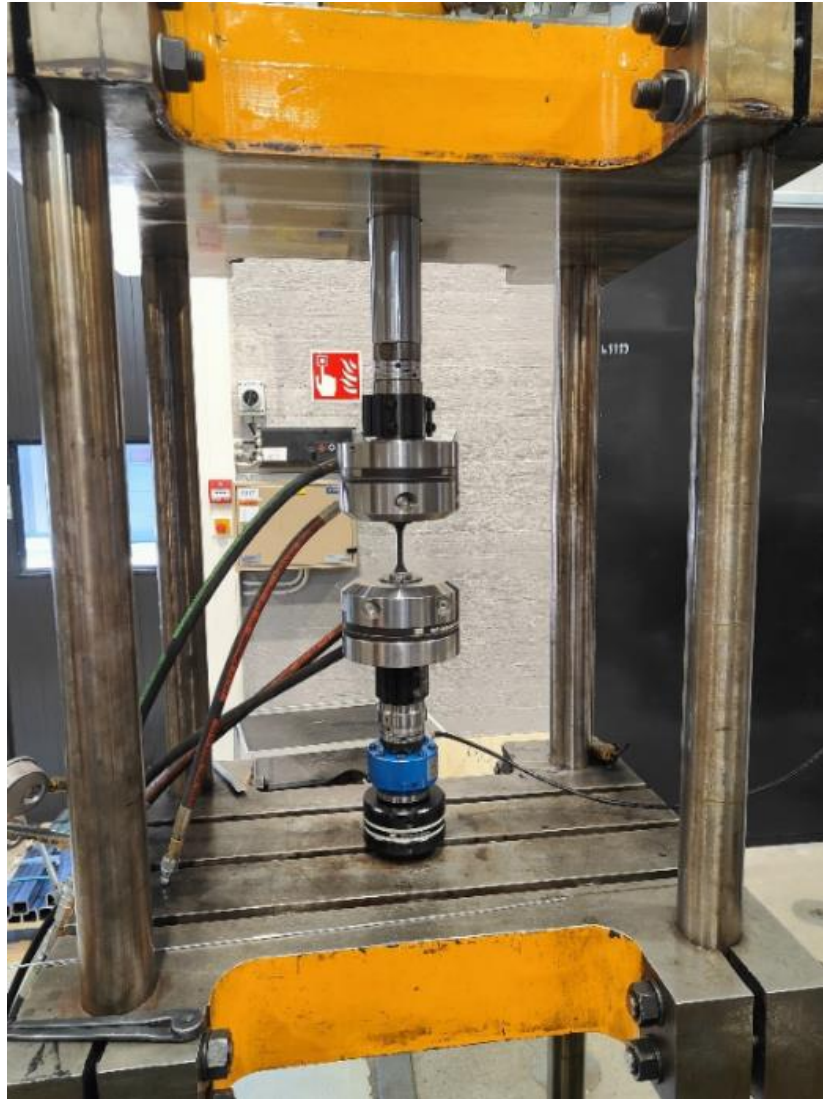


Figure 10. Fatigue test setup for WAAM X96 specimens.

Table 2. This table shows the loading for each fatigue test, where F_a is the loading amplitude, F_R is the loading range and area is the cross-section area of the test specimen.

Specimen	$F_a = \frac{(F_{max} - F_{min})}{2}$	F_{max}	F_{min}	$F_R = F_{max} - F_{min}$	Area
F-X96-AB-1	8.95 kN	18 kN	0.1 kN	17.9	36mm ²
F-X96-AB-2	7.95 kN	16 kN	0.1 kN	15.9	36mm ²
F-X96-AB-3	6.95 kN	14 kN	0.1 kN	13.9	36mm ²
F-X96-AB-4	5.45 kN	11 kN	0.1 kN	10.9	36mm ²
F-X96-AB-5	4.45 kN	9 kN	0.1 kN	8.9	36mm ²
F-X96-AB-6	3.45 kN	7 kN	0.1 kN	6.9	36mm ²

4.6 S-N curves

S-N curves were made for analyzing the fatigue test results. The fatigue test results, and S-N curves were fitted onto a log-log plot, where the vertical S-axis contains the stress range values and the horizontal N-axis contains the number of cycles. Two different S-N curves were made with Microsoft Excel to fit the fatigue test results, where the first was calculated using equations 10 to 17 with a fixed slope of $m = 3$ as recommended for welded structures (Hobbacher, 2016) and the second curve was fitted onto the results using Excel's "Power" trendline. The calculations were derived from Basquin's Law described by equation 9.

$$\Delta\sigma^m N_f = C \quad (9)$$

$$\rightarrow m \log(\Delta\sigma) + \log(N_f) = \log(C) \quad (10)$$

Where $\Delta\sigma$ is the cyclic stress range, C is the fatigue strength coefficient and N_f is the number of cycles till failure. Firstly, the cyclic stress range values $\Delta\sigma_i$ and number of cycles to failure N_i were transformed into their logarithmic values for each test.

$$x_i = \log(\Delta\sigma_i) \quad (11)$$

$$y_i = \log(N_i) \quad (12)$$

Since the slope for the first curve was already established as $m = 3$, the fatigue strength coefficient C was then calculated as follows.

$$\log(C) = m * \frac{\sum_{i=1}^n (x_i)}{n} + \frac{\sum_{i=1}^n (y_i)}{n} \quad (13)$$

$$\rightarrow C = 10^{\log(C)} \quad (14)$$

Where n is the number of fatigue tests. After this a FAT class was calculated, which indicates the fatigue strength at two million cycles.

$$FAT = \sqrt[m]{\frac{C}{2*10^6}} \quad (15)$$

And finally, the FAT class allowed for stresses to be calculated at any given number of cycles using the following equation.

$$\Delta\sigma_N = FAT * \left(\frac{2*10^6}{N}\right)^{\frac{1}{m}} \quad (16)$$

5 Results

This section presents the results of the experimental part, which includes the results of FEA, TCD and fatigue tests.

The stress concentrations were obtained by FEA, and they can be seen in Table 3 along with the TCD based fatigue notch factors obtained by equation 3 as well as surface quality parameters. For some of the FE-models the effective stress was not highest under the highest stress concentration but beneath a different notch, which is why some FE models in Table 3 have more than one result presented, where the line “-“ indicates that it is the same as the cell above. The FE-models are labelled by first the material (X96), then the type (AB=as built) and lastly FE-models ID number.

Table 3. This table shows the results of FEA, TCD and the surface profile parameters for each FE-model.

FE-model	SCF	K_f	P_a [mm]	P_z [mm]	W_a [mm]	W_z [mm]	R_a [μm]	R_z [μm]	figure
X96-AB-1	5.08	1.57	0.179	0.941	0.167	0.841	22.82	288.7	Figure 14
-	2.98	1.85	-	-	-	-	-	-	-
X96-AB-2	4.55	1.57	0.373	1.927	0.365	1.877	32.43	274.1	Figure 15
-	3.06	1.79	-	-	-	-	-	-	-
X96-AB-3	5.79	2.19	0.225	1.190	0.215	1.084	19.30	350.3	Figure 16
X96-AB-4	4.62	1.67	0.167	0.811	0.162	0.695	20.31	157.7	Figure 17
avg.	4.35	1.77							

Figure 11 presents the SCF's at the different notches from Table 3 and it shows how they decrease when approaching the critical distance, which in Figure 11 is represented by the vertical line at 0,1mm. The figure displays how some notches have a higher SCF, but it

decreases more rapidly when approaching the critical distance, while others have a lower SCF at notch root, but the stress decreases more gradually.

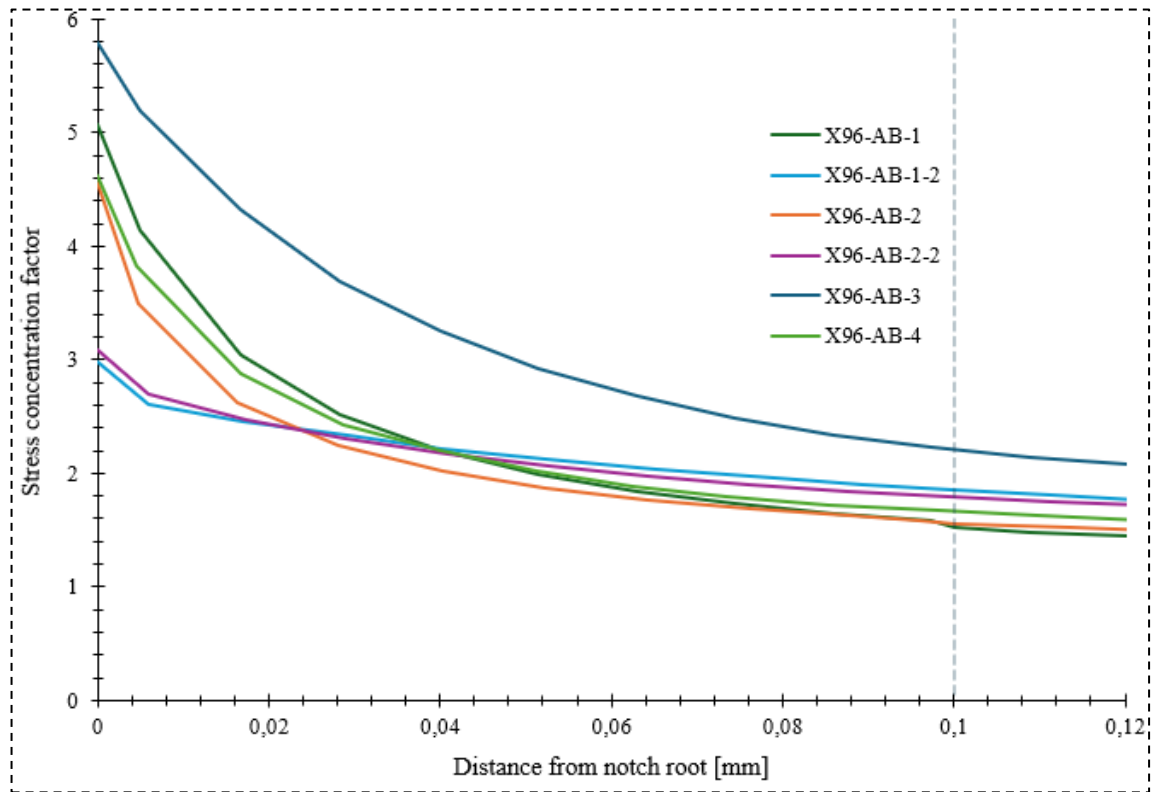


Figure 11. This figure shows the relation between SCF and distance from notch root for FEA.

The results of the fatigue tests can be seen in Table 4, which shows the applied tensile stress range for each specimen and the number of stress cycles N at which the specimens broke.

Table 4. Shows the fatigue test results, where N is the number of loading/stress cycles.

Test specimen	Stress range. [MPa]	N
F-X96-AB-1	497.22	14495
F-X96-AB-2	441.67	23146
F-X96-AB-3	386.11	38333
F-X96-AB-4	302.78	68670
F-X96-AB-5	247.22	228034
F-X96-AB-6	191.67	862609

Figure 12 shows S-N curves based on the fatigue test results shown in Table 4, where the black squared dots describe each fatigue test specimens at failure and the two lines describe estimated FAT classes with one FAT class of 110 MPa a slope of $m = 3$ as recommended for welded structures (Hobbacher, 2016) and another line with FAT class of 151 MPa and $m = 4.25$, which was fitted to the test results.

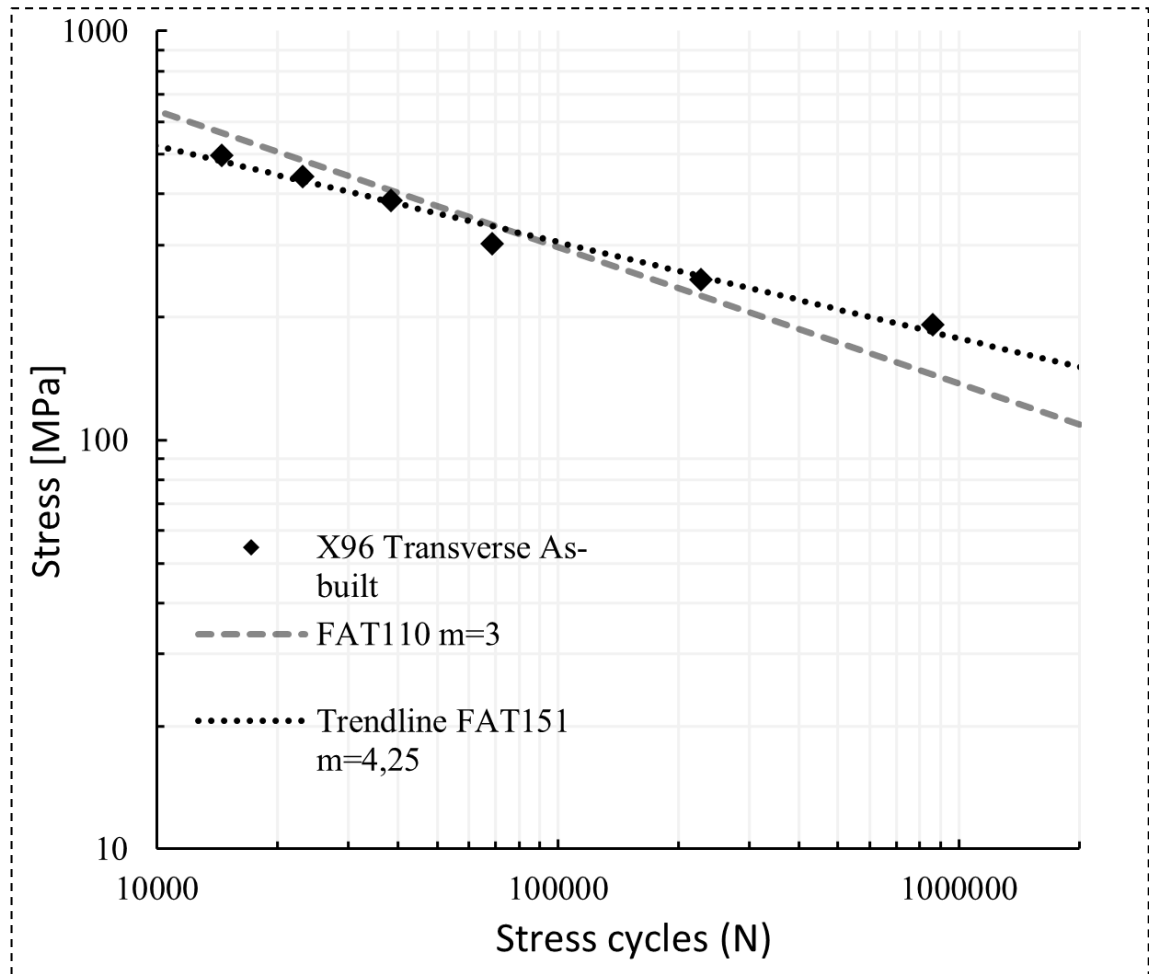


Figure 12. S-N curve shows the number of cycles to failure.

6 Discussion

This section will discuss the key results found in this thesis and they will be compared with some of the previous research that was presented in the literature review. The reliability and validity of this thesis will be also briefly evaluated in this section and the final conclusions will be drawn.

6.1 Key findings and comparison to previous research

Based on the fatigue tests done in this thesis FAT classes of 110 MPa with a slope $m = 3$ and 145 MPa with a fitted slope of $m = 4.25$ were calculated with the latter showing a more accurate fit with, however it should be noted that the 2016 IWW recommendations for welded structures by Hobbacher do not recommend calculating slopes for fatigue test series with under 10 specimens. The FEA and TCD calculations indicated an average fatigue notch factor of 1.77. The FEA and TCD results also showed that the highest fatigue notch factor was not always found under the highest peak stress, which may indicate that some small and sharp notches with higher stress peaks that were located in either a less wavy area or not quite at the root of a wavelike undulation were not as critical as some smoother area located at the root of a larger wave like undulations where the peak stress was lower but the stress decreased less rapidly towards the critical distance when compared to the sharp small notches where the stress decreased more rapidly towards the critical distance.

The results from the finite element analysis and fatigue tests can be compared with the 2023 study by Hensel et al., where the fatigue strength of WAAM components fabricated in different built positions was evaluated using finite element analysis, a local effective notch stress approach, and fatigue tests. A high-strength filler wire was used in their research ($R_{p0.2} = 820$ MPa as listed by the manufacturer), which is comparable to the filler wire used in this thesis ($R_{p0.2} = 930$ MPa). Hensel et al.'s effective notch stress approach yielded average effective notch factors of 1.5 and 1.7 for the specimens fabricated in a vertical 0-degree build position. These factors were derived by dividing the effective stress by the nominal stress. Although this thesis employed a different method to determine the effective stress, the effective notch factors from Hensel et al.'s research can be compared with the

fatigue notch factors used in this thesis, which averaged at 1.77. Furthermore, the fatigue tests conducted in both studies can also be compared, where Hensel et al.'s research resulted in a FAT160 and slope of $m=4$, while this thesis yielded a FAT151 and a slope of $m=4.25$. Despite the slight differences, these results provide a good comparison between the two studies. Also, given that the base material strength in this thesis was higher than that in Hensel et al.'s research, yet resulted in a lower FAT class, it makes sense to expect higher fatigue notch factors for this study. It is important to also note that there may be other contributing factors which may affect the difference in results for example a difference in component fabrication resulting in a difference in part or surface quality or a difference in how the fatigue tests were employed.

Another comparable study is by Huang et al. in 2023 where fatigue tests were used as well as finite element analysis along with other numerical calculations to evaluate the fatigue performance of WAAM components. The numerical analysis in Huang et al. research resulted in fatigue notch factors averaging at about 1.74, which is comparable to the 1.77 obtained in this thesis, where again both factors were obtained through different numerical approaches.

6.2 Reliability and validity

This study used a sample size of six test specimens for the fatigue tests and while it gave reasonable results, a limited sample size may introduce variability in the results, reducing the reliability of the findings. Also, a larger sample size of at least ten would be required for the statistical evaluation and error analysis of the results. The finite element analysis in this study was based on four different models. While these models provided valuable insights, incorporating a larger number of models could offer a more accurate representation of surface quality and allow for more comprehensive statistical evaluation. Also fatigue tests with machined versions of the X96 WAAM parts would be useful to compare how accurate the FEA and TCD results were.

Regarding validity, the FEA captured how surface quality caused stress concentrations in the component, which aligns with the evaluation of the effects of surface quality on the fatigue performance of WAAM components. It is however important to note that for the fatigue tests, the fatigue performance can be influenced by factors beyond surface quality,

such as residual stresses and other welding defects. While these factors were not the focus of this study, they could potentially affect the results.

6.3 Conclusions

This thesis investigated the fatigue behavior of WAAM components including an experimental part evaluating the fatigue performance of high strength X96 WAAM with the use of FEA, TCD and fatigue tests. The literature review found WAAM to be a promising technology in several industries however it was also clearly seen that the poor surface quality of as-built WAAM components caused a significant decrease in their fatigue performance. Based on the fatigue tests the as-built X96 WAAM components were given FAT classes of 151MPa with a slope of $m=4.25$ and 110MPa with a slope of $m=3$. The surface undulations of the as-built test specimens caused high local stress concentrations which were seen in the finite element analysis and the TCD found fatigue notch factors to be on average 1.77 which coincides with some of the previous research and may support FEA and TCD point method to be a useful tool for evaluating fatigue performance of WAAM components. More research would however be needed, possibly evaluating the fatigue notch factors by comparing as-built components with machined components. Overall, this thesis provided useful results on both the fatigue strength of WAAM components and how surface quality may affect it as well as insight on the use of FEA and TCD for fatigue strength evaluation of WAAM components.

References

Afkhami, S., Amraei M, Unt A, Piili H and Björk T, (2021) Metal Additive Manufacturing for Industrial Applications.: LUT University.

Bartsch H, Kühne R, Citarelli S, Schaffrath S and Feldmann M (2021) Fatigue analysis of wire arc additive manufactured (3D printed) components with unmilled surface. Structures (Oxford) 31: 576-589.

Bathias C and Pineau A (2010) Fatigue of Materials and Structures. London: ISTE.

Becker TH, Kumar P and Ramamurty U (2021) Fracture and fatigue in additively manufactured metals. Acta Materialia 219: 117240.

Cunningham CR, Wikshåland S, Xu F, Kemakolam N, Shokrani A, Dhokia V and Newman ST (2017) Cost Modelling and Sensitivity Analysis of Wire and Arc Additive Manufacturing. Procedia Manufacturing 11: 650-657.

Dirisu P, Supriyo G, Martina F, Xu X and Williams S (2020) Wire plus arc additive manufactured functional steel surfaces enhanced by rolling. International Journal of Fatigue 130: 105237.

Dutta B, Babu S and Jared BH, (2019) Science, Technology and Applications of Metals in Additive Manufacturing. San Diego: Elsevier.

Evans SI, Wang J, Qin J, He Y, Shepherd P and Ding J (2022) A review of WAAM for steel construction – Manufacturing, material and geometric properties, design, and future directions. Structures (Oxford) 44: 1506-1522.

Gardner L (2023) Metal additive manufacturing in structural engineering – review, advances, opportunities and outlook. Structures (Oxford) 47: 2178-2193.

Gockel J, Sheridan L, Koerper B and Whip B (2019) The influence of additive manufacturing processing parameters on surface roughness and fatigue life. *International Journal of Fatigue* 124: 380-388.

Hensel J, Müller J, Scharf-Wildenhain R, Uhlenberg L and Hälsig A (2023) The effects of building position on surface and fatigue of DED-arc steel components. *Welding in the World* 67(4): 859-872.

Hietala M, Rautio T, Jaskari M, Pakkila J, Keskitalo Mand Jarvenpaa A, (2023) The Influence of Surface Quality on Fatigue Strength of Wire Arc Additive Manufactured 316L Stainless Steel.: IEEE 99-103.

Hobbacher AF (2016) *Recommendations for Fatigue Design of Welded Joints and Components*. : Springer.

Huang C, Li L, Pichler N, Ghafoori E, Susmel L and Gardner L (2023) Fatigue testing and analysis of steel plates manufactured by wire-arc directed energy deposition. *Additive Manufacturing* 73: 103696.

Karakaş Ö, Leitner M and Tüzün N (2022) Application of critical distance approach for fatigue assessment of welded and HFMI-treated steel joints. *International Journal of Fatigue* 154: 106534.

Lin Z, Song K and Yu X (2021) A review on wire and arc additive manufacturing of titanium alloy. *Journal of Manufacturing Processes* 70: 24-45.

Lipiäinen K, Ahola A, Kaijalainen A and Björk T (2022) Fatigue performance of notched and hot-dip galvanized laser and mechanically cut S960 steel components considering local defects with the theory of critical distances. *International Journal of Fatigue*.

Martina F, Ding J, Williams S, Caballero A, Pardal G and Quintino L (2019) Tandem metal inert gas process for high productivity wire arc additive manufacturing in stainless steel. *Additive Manufacturing* 25: 545-550.

Murakami Y (2019) Metal Fatigue : Effects of Small Defects and Nonmetallic Inclusions. : London.

Nussbaumer A, Borges L and Davaine L, (2018) Fatigue Design of Steel and Composite Structures: Eurocode 3: Design of Steel Structures, Part 1-9 Fatigue, Eurocode 4: Design of Composite Steel and Concrete Structures. Newark: WILEY.

Pant H, Arora A, Gopakumar GS, Chadha U, Saeidi A and Patterson AE (2023) Applications of wire arc additive manufacturing (WAAM) for aerospace component manufacturing. International Journal of Advanced Manufacturing Technology 127(11-12): 4995-5011.

Pilkey DF, Pilkey WD and Bi Z, (2020) Peterson's Stress Concentration Factors. Hoboken, NJ: Wiley.

Salunkhe S, Amancio-Filho S and Davim JP, (2023) Advances in Metal Additive Manufacturing. Cambridge, Massachusetts: Woodhead Publishing.

Sandeep KJ, Teja PJ, Choudhary AK and Jain R (2022) Development of correlation between temperature, liquid life span, molten pool, and porosity during Wire Arc Additive Manufacturing: A finite element approach. CIRP Journal of Manufacturing Science and Technology 38: 274-287.

SFS-EN ISO 4287:1997, Geometrical product specifications (GPS). Surface texture: Profile method. Terms, definitions and surface texture parameters.

SFS-EN ISO 16610-21:2011, Geometrical product specifications (GPS). Filtration. Part 21: Linear profile filters: Gaussian filters.

SFS-EN ISO 21920-2:2022, Geometrical product specifications (GPS). Surface texture: Profile – Part 2: Terms, definitions and surface texture parameters.

SFS-EN ISO 21920-3:2022, Geometrical product specifications (GPS). Surface texture: Profile – Part 3: Specification operators.

SFS-EN ISO/ASTM 52900:2021, Additive manufacturing — General principles —
Fundamentals and vocabulary

Shah A, Aliyev R, Zeidler H and Krinke S (2023) A Review of the Recent Developments and Challenges in Wire Arc Additive Manufacturing (WAAM) Process. *Journal of Manufacturing and Materials Processing* 7(3): 97.

Shamir M, Zhang X, Syed AK and Sadler W (2023) Predicting the Effect of Surface Waviness on Fatigue Life of a Wire + Arc Additive Manufactured Ti-6Al-4V Alloy. *Materials* 16(15): 5355.

Singh R (2016) *Applied Welding Engineering : Processes, Codes, and Standards*. Amsterdam, Netherlands: Butterworth-Heinemann.

Tomar B, Shiva S and Nath T (2022) A review on wire arc additive manufacturing: Processing parameters, defects, quality improvement and recent advances. *Materials Today Communications* 31: 103739.

Voestalpine Böhler Welding, Solid Wires. [Online] [Retrieved 15.3.2024] available at: <https://www.voestalpine.com/welding/global-en/products/product-search/solid-wires/#LowAlloySteel4>

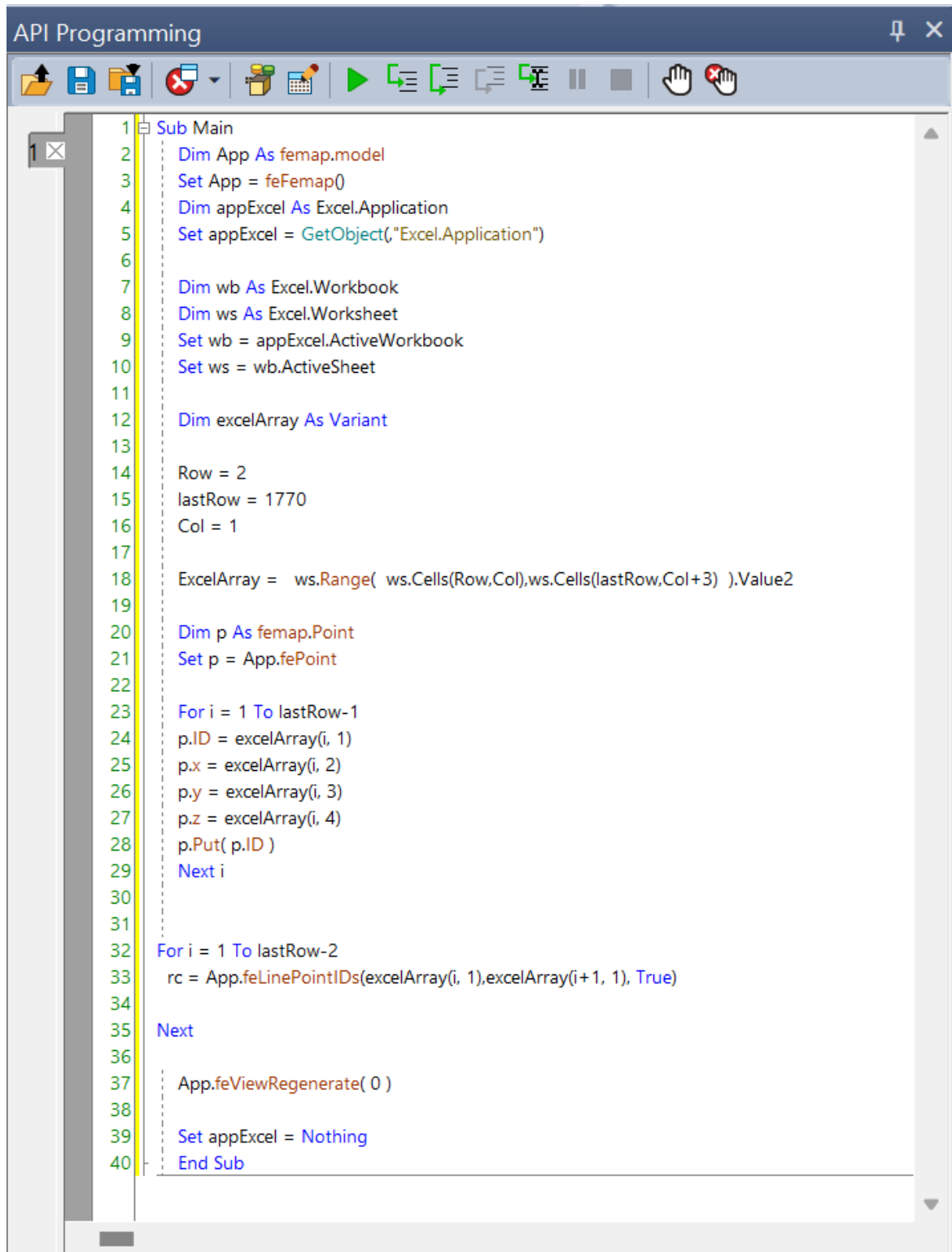
Wu B, Pan Z, Ding D, Cuiuri D, Li H, Xu J and Norrish J (2018) A review of the wire arc additive manufacturing of metals: properties, defects and quality improvement. *Journal of Manufacturing Processes* 35: 127-139.

Zhang G (2012) Method of effective stress for fatigue: Part I – A general theory. *International Journal of Fatigue* 37: 17-23.

Ziółkowski Mand Dyl T (2020) Possible Applications of Additive Manufacturing Technologies in Shipbuilding: A Review. *Machines (Basel)* 8(4): 84.

3D Printed Stainless Steel Bridge. [MX3D] Retrieved [Feb 15, 2024] Available at: <https://mx3d.com/industries/mx3d-bridge/>

Appendix 1: The code used in FEMAP API to import the surface profile data.



```
1 Sub Main
2   Dim App As femap.model
3   Set App = feFemap()
4   Dim appExcel As Excel.Application
5   Set appExcel = GetObject("Excel.Application")
6
7   Dim wb As Excel.Workbook
8   Dim ws As Excel.Worksheet
9   Set wb = appExcel.ActiveWorkbook
10  Set ws = wb.ActiveSheet
11
12  Dim excelArray As Variant
13
14  Row = 2
15  lastRow = 1770
16  Col = 1
17
18  ExcelArray = ws.Range( ws.Cells(Row,Col),ws.Cells(lastRow,Col+3) ).Value2
19
20  Dim p As femap.Point
21  Set p = App.fePoint
22
23  For i = 1 To lastRow-1
24    p.ID = excelArray(i, 1)
25    p.x = excelArray(i, 2)
26    p.y = excelArray(i, 3)
27    p.z = excelArray(i, 4)
28    p.Put( p.ID )
29  Next i
30
31
32  For i = 1 To lastRow-2
33    rc = App.feLinePointIDs(excelArray(i, 1),excelArray(i+1, 1), True)
34
35  Next
36
37  App.feViewRegenerate( 0 )
38
39  Set appExcel = Nothing
40 End Sub
```

Figure 13. The FEMAP API code used to import surface profiles from excel to FEMAP.

Appendix 2: FEA models.

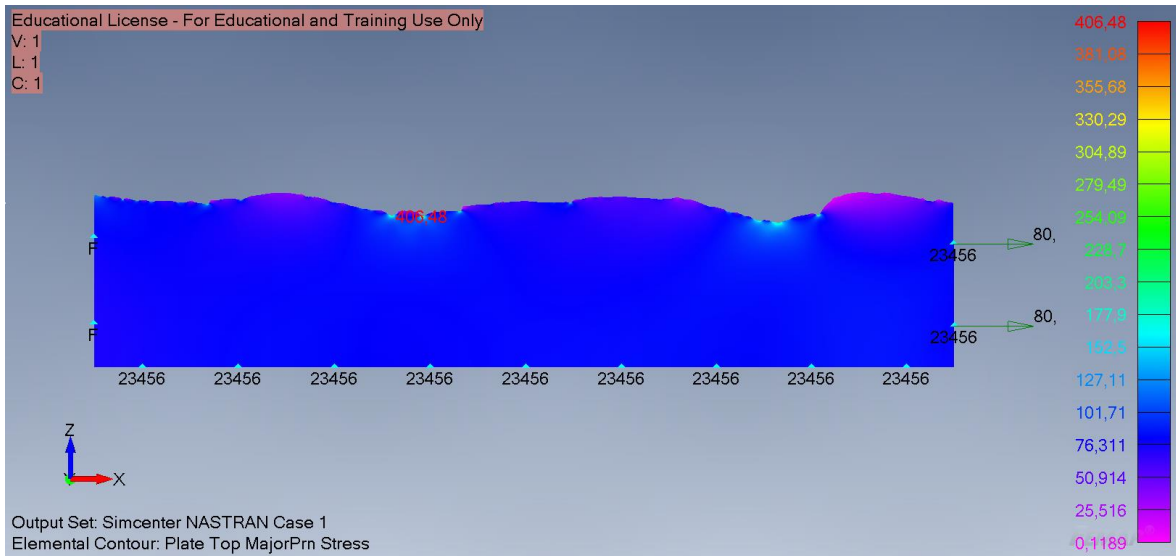


Figure 14. FEA model X96-AB-1.

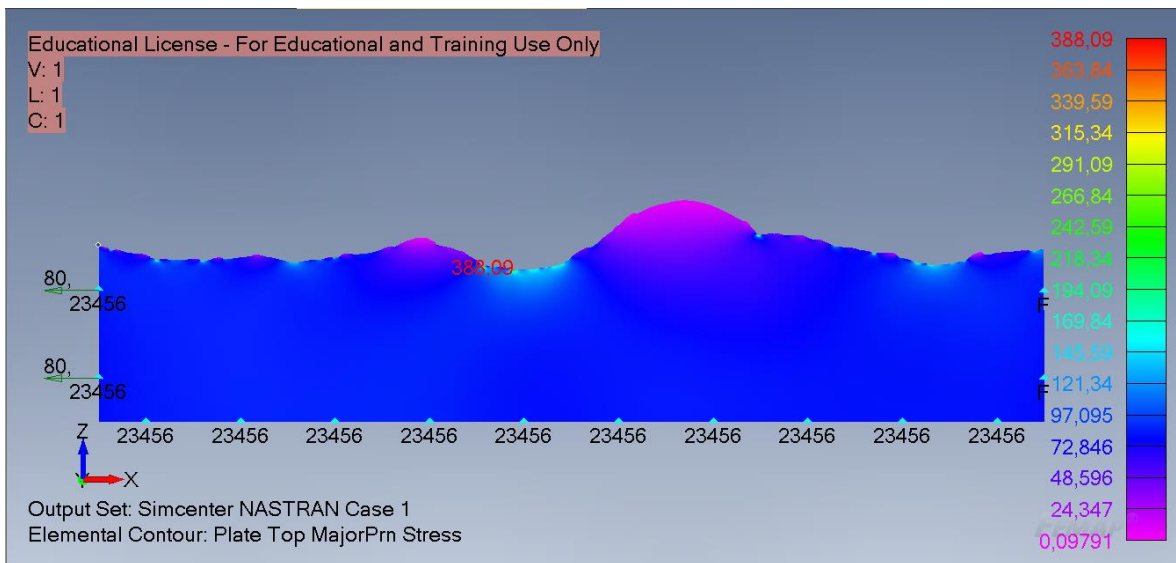


Figure 15. FEA model X96-AB-2.

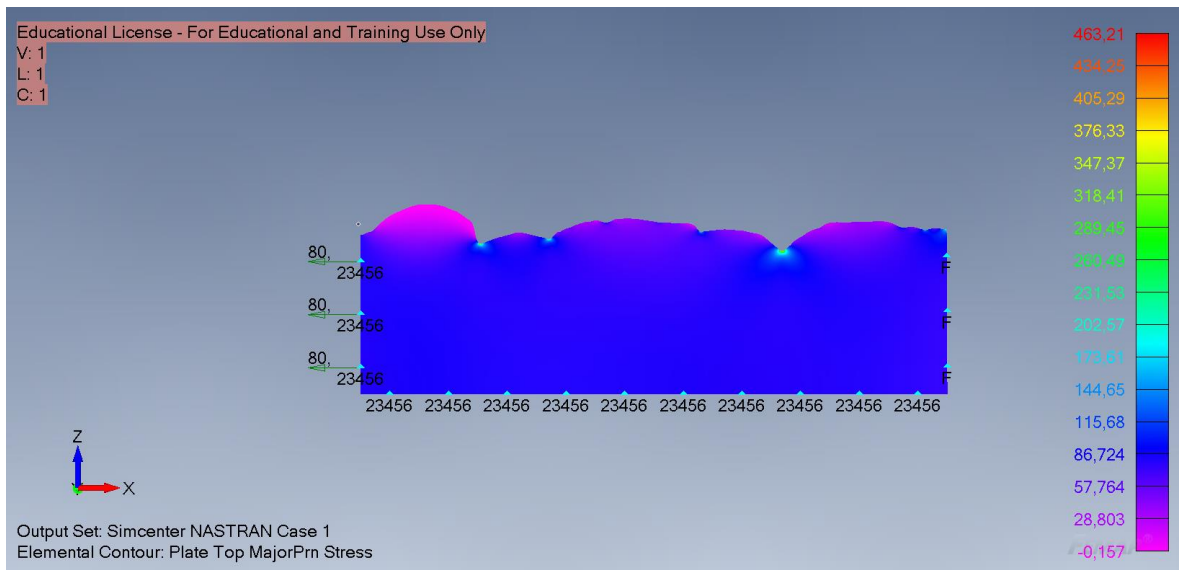


Figure 16. FEA model X96-AB-3.

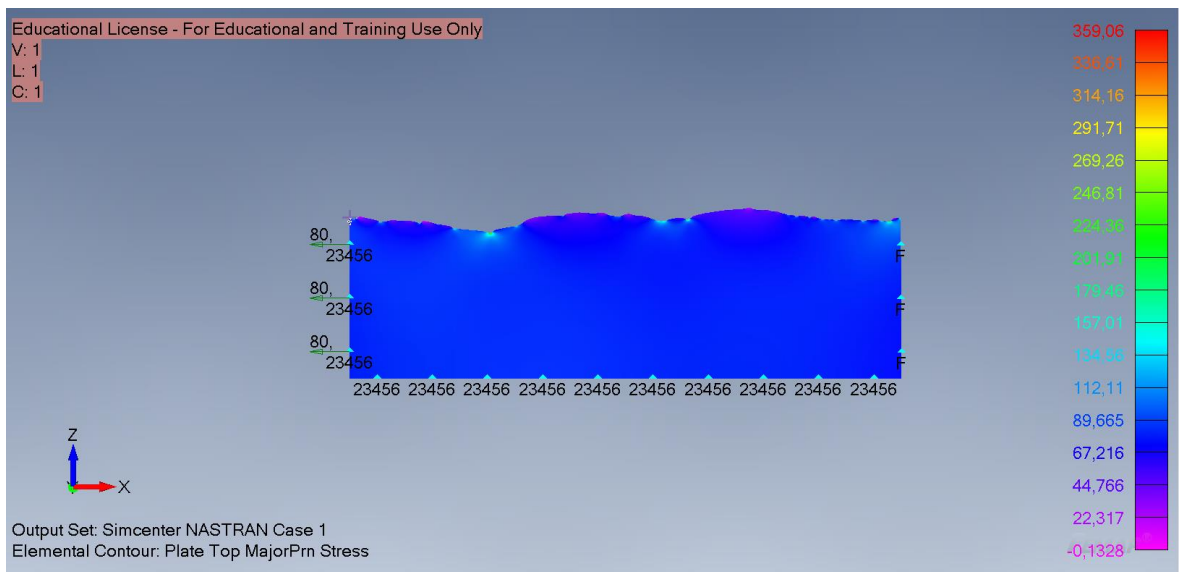


Figure 17. FEA model X96-AB-4.